ACS Biomaterials SCIENCE & ENGINEERING

Article

pubs.acs.org/journal/abseba

Micro- and Ultrastructural Characterization of Age-Related Changes at the Anterior Cruciate Ligament-to-Bone Insertion

Dovina Qu,[†] Philip J. Chuang,[†] Sagaw Prateepchinda,[†] Priya S. Balasubramanian,[‡] Xinwen Yao,[‡] Stephen B. Doty,[§] Christine P. Hendon,[‡] and Helen H. Lu*[,†]

[†]Biomaterials and Interface Tissue Engineering Laboratory, Department of Biomedical Engineering, Columbia University, 1210 Amsterdam Avenue, 351 Engineering Terrace, MC 8904, New York, New York 10027, United States

[‡]Structure−Function Imaging Laboratory, Department of Electrical Engineering, Columbia University, 500 W. 120th Street, 1300 S. W. Mudd Building, MC 4712, New York, New York 10027, United States

[§]Analytical Microscopy Laboratory, Hospital for Special Surgery, 535 East 70th Street, New York, New York 10021, United States

ABSTRACT: There remains a lack of understanding of the structural changes that occur across the complex, multitissue anterior cruciate ligament (ACL)-to-bone insertion as a function of aging. The objective of this study is to provide a multiscale comparison of matrix properties across the skeletally immature and mature ACL-to-bone insertion. Using complementary imaging methods, micro- and ultrastructural analysis of the insertion revealed that collagen fiber orientation at the interface changes with age, though the degree of collagen organization is maintained over time. These changes are accompanied by a decrease in collagen fibril density and are likely driven by physiological loading. Mineral crystal structure and crystallinity are conserved over time, despite regional differences in crystallinity between the interface and bone. This suggests that mineral chemistry is established early in development and underscores its important functional role. Collectively, these findings provide new insights into interface development and set critical design benchmarks for integrative soft tissue repair.

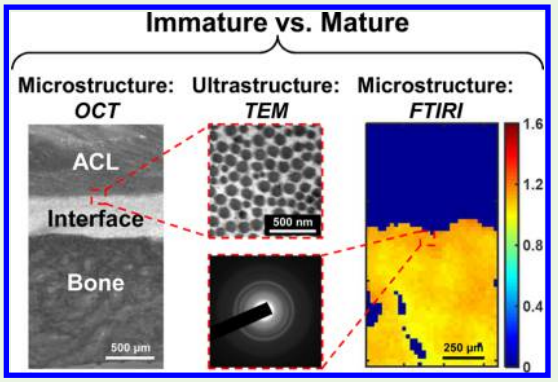

KEYWORDS: *insertion, interface, aging, ligament, collagen, mineral*

INTRODUCTION

The integration of compositionally and mechanically dissimilar tissues through complex biological interfaces is critical for musculoskeletal function. Among these interfaces, the junctions where the anterior cruciate ligament (ACL) attaches to bone are especially important. As the primary stabilizer of the knee,[1] the ACL connects the femur and tibia and inserts into either bone via a fibrocartilaginous enthesis, which can be further divided into nonmineralized and mineralized regions.[2,3] The nonmineralized fibrocartilage is contiguous with the ligament and consists of rounded fibrochondrocytes embedded in a type I and II collagen-rich, proteoglycan-containing matrix,[4,5] and the adjacent mineralized fibrocartilage is contiguous with bone and consists of hypertrophic chondrocyte-like cells within a mineralized matrix.[6,7] These regional differences in matrix composition contribute to graduated changes in mechanical properties[8] which serve to reduce the formation of stress concentrations and mediate load transfer between the ligament and bone.[2,3]

However, the complex ligament-to-bone transition is not re-established following ACL reconstruction, which compromises long-term graft stability and function.[9−11] As the ACL is the most frequently injured ligament of the knee,[12] there is significant clinical interest in methods for regeneration of this functional interface. In particular, an understanding of the micro- and ultrastructural properties of the native ACL-to-bone insertion is essential for establishing the much needed benchmark parameters for integrative and functional ACL reconstruction, as well as current approaches in ligament repair[13] and regeneration.

The ACL-to-bone insertion has been closely studied using conventional histology and light microscopy methods,[1−3,5,7,14,15] which have shown that organized collagen fibers from the ligament persist across the insertion into the bone and that mineral is localized to the calcified fibrocartilage and bone regions. However, quantitative and ultrastructural characterization of matrix properties remains challenging due to the structural complexity and relatively short length scale of the enthesis.[1,2,7,16] In this study, several complementary imaging and analysis methods are applied to examine the micro- and ultrastructural properties of the ACL-to-bone insertion. Optical coherence tomography (OCT) provides depth resolved, three-

Special Issue: Multiscale Biological Materials and Systems: Integration of Experiment, Modeling, and Theory

Received: September 30, 2016
Accepted: November 13, 2016

DOI: 10.1021/acsbiomaterials.6b00602
ACS Biomater. Sci. Eng. XXXX, XXX, XXX−XXX

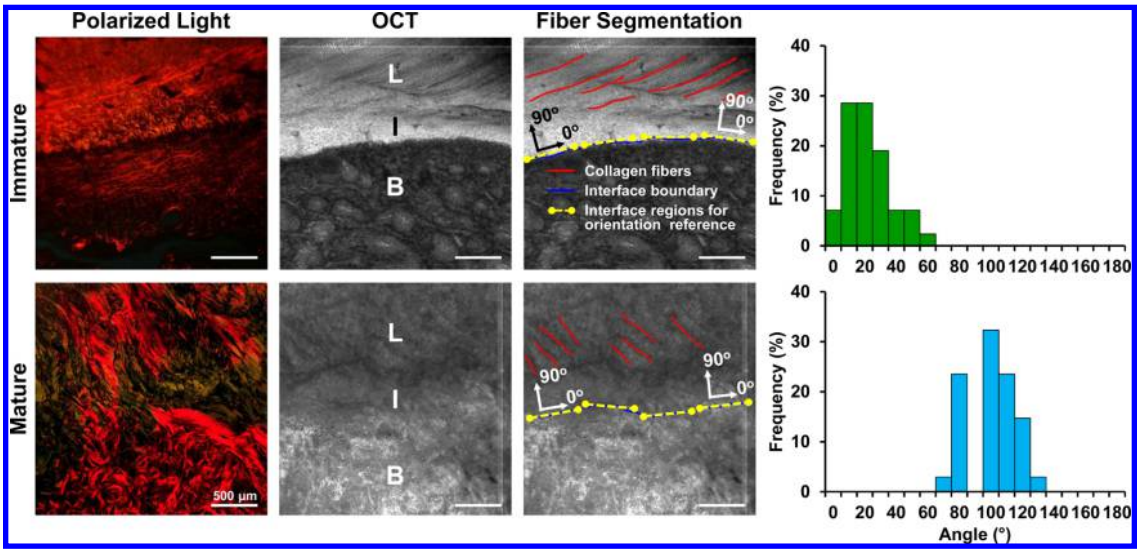

Figure 1. Analysis of collagen organization by OCT. Collagen fiber orientation was visualized in polarized light images of Picrosirius red-stained sections and by OCT. Three-dimensional OCT imaging data sets are displayed as sum projections within representative immature and mature ACL-to-bone insertion samples (L, ligament; I, interface; B, bone). Collagen fibers are visible within the ligament regions, and the angle of fibers relative to the interface were measured from images at a fixed distance within each volume (n = 4/group). While fiber angles are primarily oriented near parallel to the ligament-to-bone interface in immature samples, insertion angles are nearly perpendicular in mature samples.

dimensional imaging of biological tissue at video rate with micron-scale resolution[17] and can be used to characterize microstructural features such as fiber architecture in fresh, unfixed tissues.[18−21] Vibrational spectroscopy techniques such as Fourier transform infrared spectroscopy imaging (FTIRI) provide a method to generate quantitative, micron-resolution spatial maps of physicochemical properties such as tissue composition and mineral crystallinity, and have been shown to correlate well with traditional biochemical and histological analyses.[22−24] Complementary to these microscale analysis techniques, transmission electron microscopy (TEM) allows for the examination of tissue ultrastructure. Structural information such as morphology and particle size can be obtained from TEM in imaging mode, while analysis of crystal structure can be determined in diffraction mode. Note that TEM has been used extensively to study the ultrastructure of cells and tissues, including the ACL.[25,26]

Age-related changes in ACL healing potential,[27,28] mechanical properties,[29,30] as well as structural and compositional changes at the insertion[7,31] have been observed. As ACL injuries occur in patients of all ages, with the incidence of injury in patients aged 40 and older increasing in particular,[32] it is critical to develop a more thorough understanding of age-related differences at the insertion for more effective and personalized ACL repair strategies. Therefore, the objective of this study is to characterize and compare the micro- and ultrastructural properties of the ACL-to-bone insertion in skeletally immature and mature specimens using OCT, FTIRI, and TEM. Combining classic and novel functional imaging methods, this study tests the hypothesis that in addition to spatial differences in collagen matrix architecture and mineral chemistry, these interface properties will also change as a function of age. The bovine ACL model was selected for this study as it exhibits structural resemblance to human anatomy[33] and has been well characterized,[7,8,34,35] enabling multimodal characterization in a readily accessible and reproducible model. On the basis of previous single-tissue (ligament, fibrocartilage, or bone only) studies on age-related changes,[7,26,31,36−41] it is expected that mineral chemistry, matrix collagen density, and organization will increase with age, while maintaining spatial differences across the multitissue ACL enthesis.

MATERIALS AND METHODS

Sample Isolation. Bovine tibiofemoral joints were obtained from a local abattoir (Green Village Packing Company) and were divided into two age groups: immature (4 to 6 months old) and mature (2 to 5 years old). Following removal of the surrounding muscle, subcutaneous fascia, collateral ligaments, patella, patellar tendon, adipose tissue, and menisci, the femoral and tibial ACL insertions were identified and excised. Each sample comprised the ligament with intact insertion connected to the bone. Collagen microstructure and mineral distribution and crystallinity were analyzed using OCT and FTIRI, respectively, while TEM was used to examine collagen matrix and mineral ultrastructure.

OCT Sample Preparation, Acquisition, and Analysis. For analysis of collagen fiber organization using OCT, fresh tissue samples (n = 4/group) were maintained in PBS and imaged within 24 hours of isolation. Optical coherence tomography image data sets (n = 4/group) were acquired at 1300 nm using a commercial spectral domain OCT system (TELESTO, Thorabs) with axial and lateral resolutions of 6.5 and 15 μm, respectively, and an imaging range of 2.52 mm, all in air. Images were acquired at video rate, with an A-line rate of 28 kHz. Multiple three-dimensional data sets of the ACL-to-bone interface were obtained, with clear imaging up to 500 μm in depth. Images were reconstructed by processing the raw interferometric data in MATLAB (R2015a, Mathworks). For each sample, one *en face* image (fixed x−y plane at specified z-depth) was selected per volume based on clear presence of fibers. Insertion angles were manually measured with respect to the ligament-bone interface using Image-J (NIH). In each image, the ligament−bone interface was portioned into 1 mm-wide segments (denoted by yellow lines in Figure 1). The average angle of each segment of the interface was used as a reference angle for the ligament fibers measured in each region with a minimum of four fibers measured per region. Mean and standard deviation of orientation measurements normalized to the reference interface angle were calculated for the immature and mature samples to describe dominant orientation and dispersion.

Histology. For histological examination of collagen alignment, samples were fixed in 80% ethanol supplemented with 1% cetylpyridinium chloride (Sigma-Aldrich) and then demineralized in

DOI: 10.1021/acsbiomaterials.6b00602
ACS Biomater. Sci. Eng. XXXX, XXX, XXX−XXX

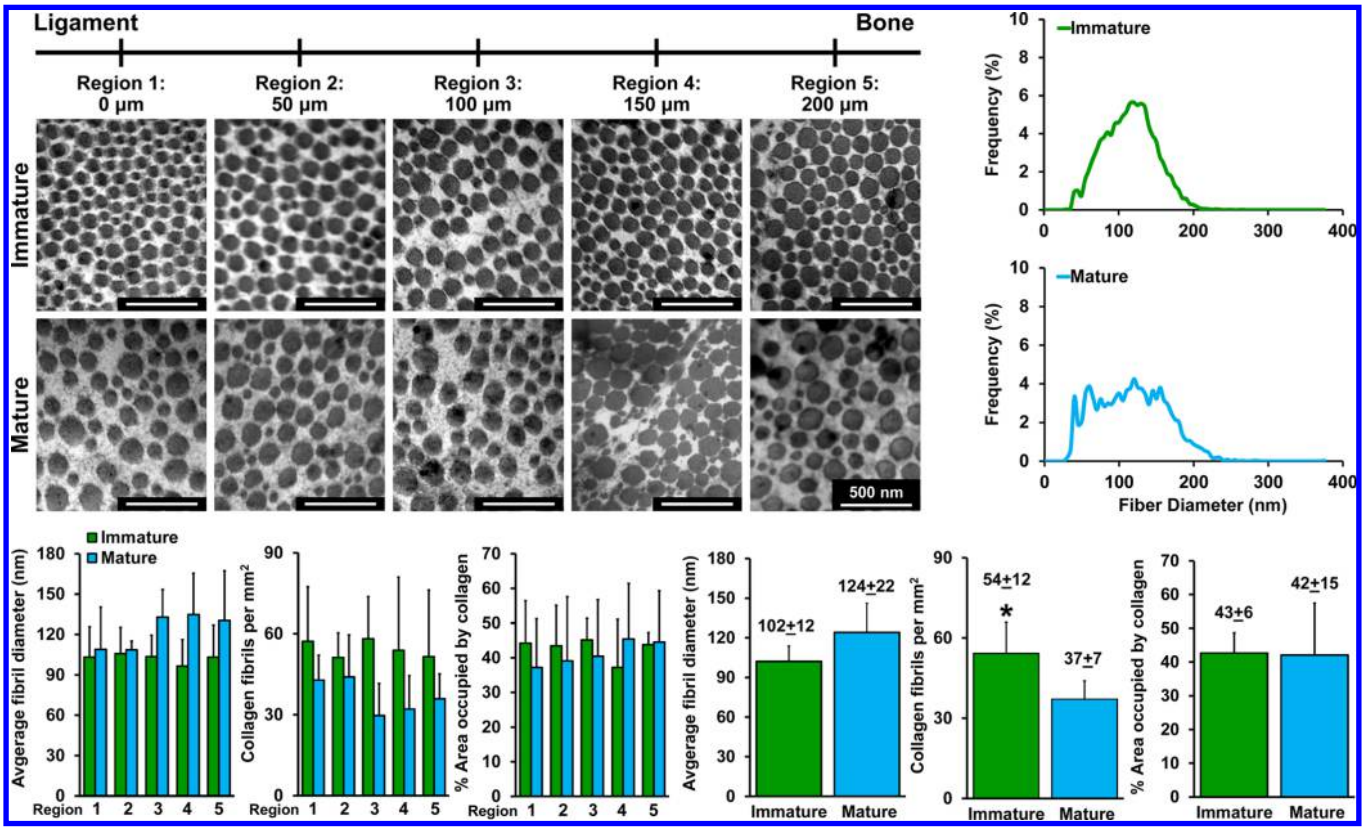

Figure 2. Collagen fibril characterization by TEM. TEM images of collagen fibrils were collected at 50 μm intervals across the ACL insertion for both immature and mature specimens (50,000×, 80 kV). Distribution of collagen fibril diameters across the insertion (n = 4) is unimodal in the immature group and multimodal in the mature group. Regional analysis of collagen fibrils revealed no significant differences in collagen fiber density (number of collagen fibers per area, n = 4), diameter (n = 4) or percent area occupied (n = 4) among ligament, non-mineralized interface, mineralized interface, and bone regions. On average, fibril density was higher in the immature interface and bone regions, while the inverse relationship was observed for fibril diameter; however, these differences were not statistically significant. Comparison of average collagen properties between immature and mature samples revealed significantly higher collagen fibril density in the immature group (n = 4, *p < 0.05), but no significant differences in fibril diameter (n = 4) or percent area occupied (n = 4) were observed.

0.05 M tris-hydroxymethylaminomethane buffer (Sigma-Aldrich, pH 7.2) containing 10% ethylenediaminetetraacetic acid (Sigma-Aldrich).[24] Samples were then dehydrated with serial concentrations of ethanol, embedded in paraffin (Fisher Scientific), and cut into 7 μm sections using a microtome (Reichert-Jung RM 2030 Microtome, Leica). Sections were collected on glass slides, dried overnight at 56 °C, cleared of paraffin in xylenes, and then stained with Picrosirius red (Sigma-Aldrich, 0.1% solution). Stained sections were imaged using a light microscope fitted with a polarized light filter (Olympus BX60, Olympus) to visualize collagen fiber organization.

FTIRI Sample Preparation, Acquisition, and Analyses. For analysis of mineral distribution and crystallinity using FTIRI, samples were fixed in 90% ethanol, dehydrated with serial concentrations of ethanol, embedded in poly(methyl methacrylate) (PMMA; Sigma-Aldrich), and then cut into 2 μm sections using a sliding microtome (SM2500S, Leica) fitted with a tungsten carbide blade (Delaware Diamond Knives).[24,34] Sections were placed immediately onto BaF_2 windows and were dried overnight at 25 °C.

Mineral distribution and crystallinity across the ACL-to-bone interface (n = 3/group) were evaluated by FTIRI. Infrared spectra were acquired using an FTIR spectrometer (Spectrum 100; PerkinElmer) coupled to a microscope imaging system (Spotlight 400; PerkinElmer).[24,34] Spectra were collected between 2000 and 800 cm^{-1} with a spectral resolution of 8 cm^{-1} and a spatial resolution of 25 μm, and were analyzed using ISYS chemical imaging software (3.1.1., Spectral Dimensions) and MATLAB (R2015b, MathWorks). To eliminate background and compensate for varying degrees of PMMA penetration into the different tissues across the interface, spectra of pure PMMA were acquired, baseline corrected, normalized by the highest peak in the PMMA spectrum (1728 cm^{-1}), and then subtracted from similarly baseline corrected and normalized sample spectra.

The relative mineral-to-matrix ratio was calculated by integrating under the ν1, ν3 phosphate band contour (1200 to 900 cm^{-1}) and dividing by the amide I band area (1720 to 1590 cm^{-1}). Mineral crystallinity was determined from the ratio of the 1030 cm^{-1} peak, which is indicative of phosphate in stoichiometric apatites, to the 1020 cm^{-1} peak, which represents nonstoichiometric apatites, with higher 1030/1020 ratios associated with more crystalline mineral.[22,42] Additionally, line profiles showing mean mineral crystallinity across the insertion were generated. Values for 100 equally spaced points spanning from ligament to bone were interpolated using a MATLAB bicubic least-squares method, allowing matrix content to be presented as a function of percent distance across the insertion, thereby accounting for any differences in fibrocartilage thickness among specimens. Average matrix values were also calculated for each tissue region (ligament, nonmineralized fibrocartilage, mineralized fibrocartilage, and bone) and compared.

TEM Sample Preparation, Acquisition, and Analysis. For TEM analysis, samples were fixed with 0.5% glutaraldehyde and 2% paraformaldehyde in 0.05 M cacodylate sodium buffer (pH 7.4) and postfixed with 1% osmium tetraoxide.[43] Samples were dehydrated with serial concentrations of ethanol, embedded in Spurr's resin, and then cut into 70−100 nm sections using a microtome (Reichert-Jung Ultracut E 701704, Leica). Sections were stained with uranyl acetate and lead citrate prior to analysis.

Collagen fibril ultrastructure across the ACL-to-bone insertion was evaluated by TEM (JEM-100CX, JEOL; 80 kV). For each sample (n =

DOI: 10.1021/acsbiomaterials.6b00602
ACS Biomater. Sci. Eng. XXXX, XXX, XXX−XXX

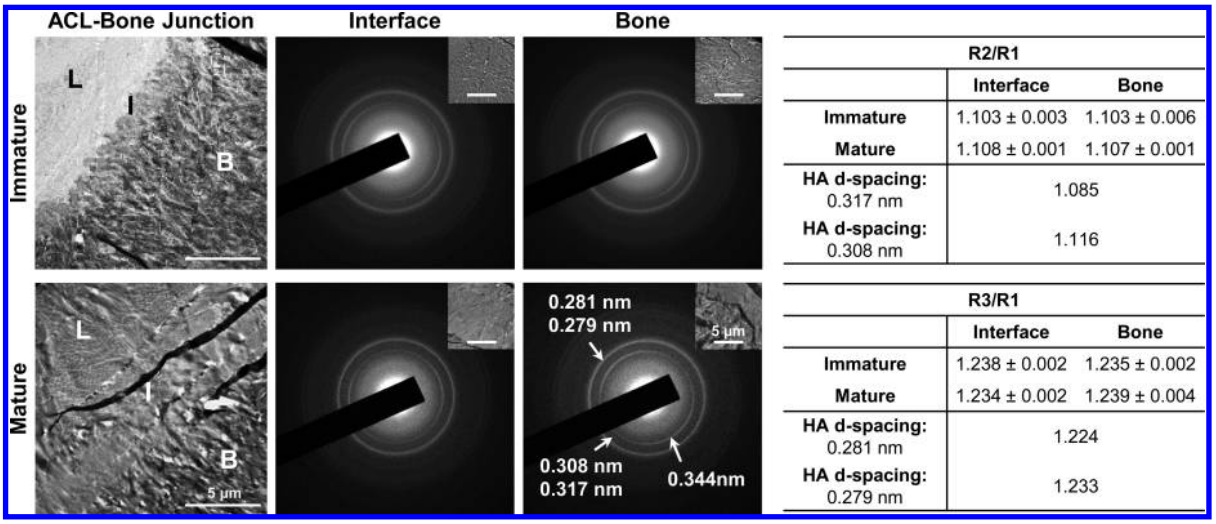

R2/R1	Interface	Bone
Immature	1.103 ± 0.003	1.103 ± 0.006
Mature	1.108 ± 0.001	1.107 ± 0.001
HA d-spacing: 0.317 nm	1.085	
HA d-spacing: 0.308 nm	1.116	

R3/R1	Interface	Bone
Immature	1.238 ± 0.002	1.235 ± 0.002
Mature	1.234 ± 0.002	1.239 ± 0.004
HA d-spacing: 0.281 nm	1.224	
HA d-spacing: 0.279 nm	1.233	

Figure 3. Mineral characterization by electron diffraction. Mineral at the ACL-to-bone insertion was characterized by electron diffraction (120 kV; camera length, 50 cm) into immature and mature samples (n = 3/group). The presence of hydroxyapatite was confirmed for all samples by indexing the diffraction rings to known d-spacings for hydroxyapatite (ICDD).

4/group), after first identifying the insertion site, images were collected starting from the bone and progressing in 50 μm increments toward the ligament region. In short, the total distance imaged spans across the insertion from ligament to nonmineralized interface, mineralized interface, and bone. A minimum of five images were collected for each region, and collagen fibril diameter, distribution, and total area were determined using Photoshop (CS5, Adobe) and Image-J (NIH).

Crystal structure (n = 3/group) in the mineralized interface and bone regions were evaluated by electron diffraction with TEM (JEM-1400, JEOL; 120 kV; camera length, 50 cm). Diffraction rings were indexed to crystal planes by measuring the radii of the rings (Image-J, NIH) and correlating them to the d-spacings of hydroxyapatite (International Centre for Diffraction Data (ICDD)),[44] assuming the first ring to be (0002). Ring radii ratios are inversely proportional to the ratio of d-spacings via Bragg's law.[45] The average horizontal and vertical radii were measured using Image-J (NIH), and the ratios of rings 2 and 3 to ring 1 were calculated based on the d-spacings and compared with those of hydroxyapatite.[44]

Statistical Analysis. Results are presented as the mean ± standard deviation. One-way analysis of variance (ANOVA) was performed on all qualitative data to determine region- and/or age-dependent differences in matrix properties. The Tukey–Kramer posthoc test was used for all pairwise comparisons, and statistical significance was attained at $p < 0.05$. All statistical analyses were performed using JMP IN (4.0.4, SAS Institute).

RESULTS

Collagen Matrix Organization. Evaluation of collagen matrix architecture across the ACL-to-bone interface by polarized light microscopy and OCT revealed well-organized fibers that insert into bone, which exhibited more disorganized fiber architecture compared to the ligament (Figure 1). Sum projections through the entire volume of each OCT scan showed different texture patterns within the ligament, interface, and bone regions, where the ligament region is distinguishable by visible fibers and a characteristic crimp pattern while the bone region exhibits a spongy appearance. The interface region of the immature samples exhibited high signal intensity, whereas the interface region of the mature samples appeared more texturally similar to bone and exhibited increased density, resulting in decreased image penetration.

Segmentation of fibers within the interface region revealed that the mature group (n = 4) exhibited near perpendicular fiber alignment relative to the interface, whereas the insertion angle in the immature group (n = 4) was closer to parallel to the interface. Specifically, the mean angle of insertion relative to the ligament–bone interface was 100.11° ± 15.27° in the mature group and 22.53° ± 13.48° in the immature group ($p < 0.05$, Figure 1).

Collagen Fibril Structure. Electron micrographs across the ACL-to-bone insertion revealed that the average fibril diameter across the interface was 102.2 ± 11.6 nm for the immature group (n = 4) and 124.1 ± 22.0 nm for the mature group (n = 4). There was an over 3-fold difference in variance, which is calculated as the square of the standard deviation, between the immature (135 nm) and mature (484 nm) groups. As shown in Figure 2, the majority of collagen fibrils in the immature samples ranged between 80–140 nm in diameter. In contrast, a wider range of distribution was observed for collagen fibril diameters of the mature group. Regional analysis revealed no significant differences in fibril diameter among ligament, fibrocartilage, and bone regions for either group.

Collagen fibril density (i.e., the number of fibrils per area) and percent area of each image occupied by collagen were also evaluated in this study (Figure 2). Regional comparison revealed no significant differences in fibril density or percent area occupied among ligament, fibrocartilage, and bone regions for immature or mature groups. However, on average, fibril density was higher in the interface and bone regions in the immature group, while the opposite trend was observed for fibril diameters in the same group. Overall, significantly higher fibril density was found in the immature group compared to that of the mature group ($p < 0.05$, Figure 2), while no significant differences in fibril diameter or percent area occupied were observed between groups.

Mineral Crystal Structure. Electron diffraction analysis was performed on the calcified tissue regions of the immature (n = 3) and mature (n = 3) insertions. Ring structures of mineral found at the interface and bone regions were characterized by the ring radii ratios (R2/R1, R3/R1), which were found to be similar to the d-spacing ratios for hydroxyapatite[44] in both groups (Figure 3). Diffraction patterns

DOI: 10.1021/acsbiomaterials.6b00602
ACS Biomater. Sci. Eng. XXXX, XXX, XXX–XXX

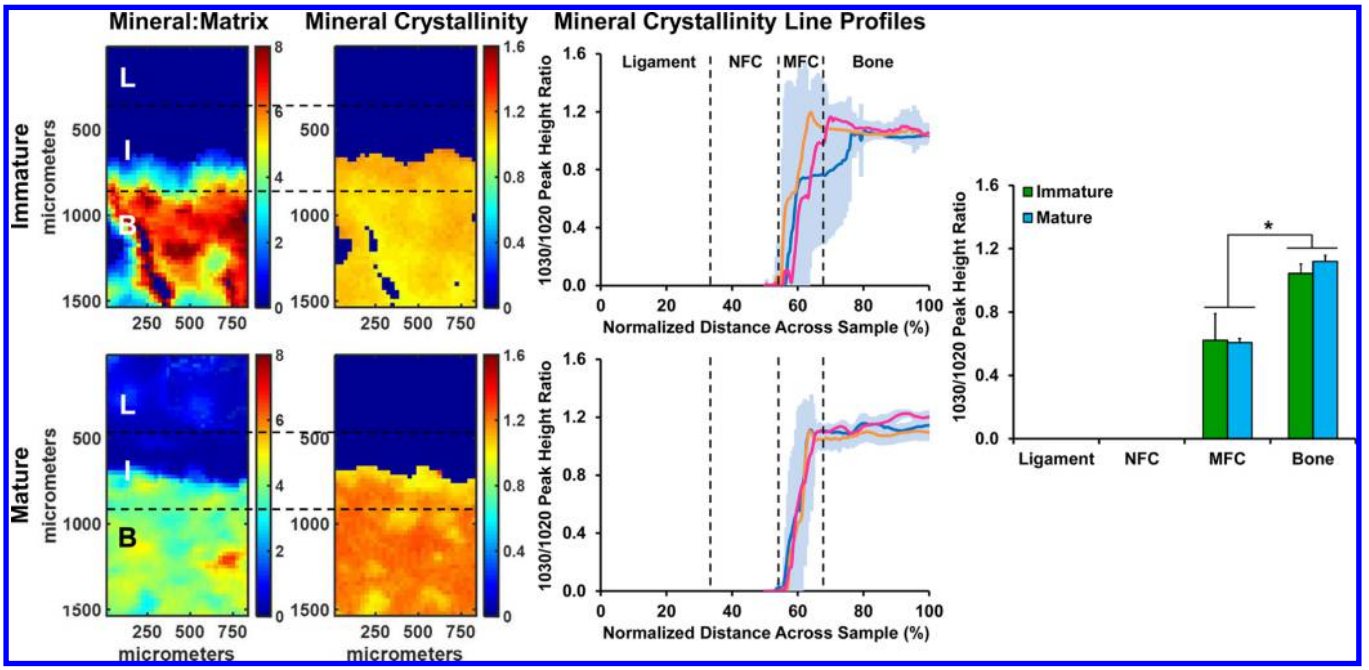

Figure 4. Analysis of mineral distribution and maturity by FTIRI. Maturity of the mineral across the immature and mature ACL-to-bone insertions (n = 3; L, ligament; NFC, nonmineralized fibrocartilage; MFC, mineralized fibrocartilage; B, bone) was determined by analysis of the 1030/1020 peak height ratio. Line scans across the interface and regression analysis of the interface (I) regions revealed a linear increase in mineral crystallinity across the MFC and significantly higher crystallinity in the bone region compared to the MFC for both immature and mature samples (blue, pink, and orange lines represent mean values from different samples, and the shaded area shows standard deviations; *p < 0.05). While the increase in mineral crystallinity across the mature interface was more linear compared to the immature interface, no significant difference in average crystallinity was observed between immature and mature samples.

were also found to be similar between regions (mineralized fibrocartilage vs bone) and between groups (immature vs mature), with no significant differences in ring ratios observed between immature and mature samples.

Mineral Distribution and Maturity. Peak integration maps of mineral-to-matrix ratio indicate that mineral content was localized to the mineralized fibrocartilage and bone regions (Figure 4). Overall relative mineral content was higher in the immature group compared to the mature group. Mineral crystallinity, as determined by the 1030/1020 peak ratio, was also assessed across the calcified tissue regions of the immature (n = 3) and mature (n = 3) insertions (Figure 4). Region-wise comparison revealed a significantly higher mean 1030/1020 ratio in the bone region (1.04 ± 0.06 for the immature group and 1.12 ± 0.04 for the mature group), compared to the mineralized fibrocartilage regions (0.62 ± 0.17 for the immature group and 0.61 ± 0.03 for the mature group) for both groups (p < 0.05, Figure 4). However, no significant differences in mineral crystallinity were observed between the immature and mature insertions.

DISCUSSION

The fibrocartilaginous ACL enthesis plays a critical role in ensuring functional ligament attachment to bone by providing a graded transition in compositional, structural, and mechanical properties between soft tissue and bone. The objective of this study was to characterize and compare micro- and ultrastructural properties of the ACL-to-bone insertion in juvenile and adult models. OCT, FTIRI, and TEM were used to analyze tissue structure at multiple scales. Age-related changes in collagenous matrix organization and structure indicate significant postnatal remodeling at the enthesis. However, mineralized matrix distribution and structural properties are highly conserved over time.

In this study, microscale evaluation of matrix structure across the ACL-to-bone enthesis showed that well-aligned collagen fibers from the ligament region insert into the fibrocartilaginous interface. Analysis of collagen fiber organization indicated that the fiber orientation changes with age, where collagen fibers are oriented approximately parallel to the interface in the immature insertion but insert perpendicularly into the interface in the mature insertion. These measurements support previous characterizations by polarized light microscopy[7] and FTIRI.[34] As collagen fibers in the tendon and ligament have been shown to realign in response to mechanical loads,[46,47] the age-related differences in fiber orientation observed here likely reflect a structural response to physiologic loads sustained by the ACL. Interestingly, however, quantitative analysis showed that the variances of the fiber orientation distributions were not different between groups, which indicates that despite the change in insertion angle over time, the degree of fiber organization is conserved over the course of development. Furthermore, it has been reported that the load needed to induce fiber realignment changes with age,[48] which suggests that changes in organization are accompanied by changes in collagen structure over time.

Indeed, analysis of collagen ultrastructure revealed significantly higher collagen fibril density in the immature insertion and correspondingly smaller fibril diameters on average, compared to that of the mature group. Moreover, the distribution of fibril size was relatively uniform in the immature group but became more disperse with age, with a 3-fold increase in variance. These findings are consistent with previous electron microscopy studies which have reported that collagen

DOI: 10.1021/acsbiomaterials.6b00602
ACS Biomater. Sci. Eng. XXXX, XXX, XXX−XXX

fibrils are smaller and unimodally distributed at birth and become larger and biomodally distributed at maturity.[49,50] These changes in fibril size and size distribution result in changes in tissue mechanical properties and are reflective of functional adaptations to physiological loads. Larger collagen fibrils are predicted to exhibit higher stiffness than smaller fibrils,[51,52] and the increased fibril size in mature tissues is likely a primary contributor to the increased stiffness and resilience of adult ligaments.[53,54] Furthermore, it has been suggested that the multimodal distribution of fibril sizes is optimized to balance functional requirements for high tensile strength and resistance to creep. While a higher number of large fibrils can enhance tensile strength by increasing the density of intrafibrillar covalent cross-links, increasing the number of smaller fibrils can improve creep inhibition by increasing the surface area per unit mass and, in turn, the density of interfibrillar electrostatic interactions.[50] Interestingly, however, Strocchi et al.[26] reported that collagen fibril diameters in the human ACL decrease with age. While previous studies have also shown that smaller fibrils are observed at senescence compared to maturity due to breakdown of fibrils and tissues with aging,[50,55] it has been shown both in this and other studies[49,50] that collagen fibril diameters are smaller in young animals than in their adult counterparts. Moreover, the animals from which immature samples were obtained in this study were much younger in equivalent human years[56] than the age range of subjects (15−87 years) in the Strocchi et al. study.

Whereas previous studies focused exclusively on the ligament proper, the present study provides the first characterization of collagen fibrils across the entire ACL-to-bone insertion. It was observed that there were no spatial differences in collagen fibril diameters across the immature interface. In contrast, collagen fiber diameters in the mature interface and bone regions were larger than those in the ligament region on average, which may be indicative of different loads sustained in each region and adaptations to these variations. Interestingly, it has also been shown that glycosaminoglycans (GAGs) are associated with the growth of smaller collagen fibrils.[57] As histological studies have shown greater GAG content at the immature interface compared to the mature interface,[7] age-dependent differences in collagen fibril diameter at the interface may be reflective of these compositional differences as well.

Mineral was found to be localized to the calcified fibrocartilage and bone regions of the ACL-to-bone enthesis. It has been shown that the graded mineralization observed at the enthesis serves to reduce stress concentrations and improve load transfer between soft tissue and bone.[58,59] Characterization of mineral chemistry across these regions by electron diffraction showed that the ring structures of mineral found at the interface and bone resemble that of hydroxyapatite (HA). Polycrystalline HA typically exhibits a distinct ring for each *d*-spacing, and in all samples, each ring ratio was found to be associated with two *d*-spacings for HA, 0.308 and 0.317 nm for R2, and 0.279 and 0.281 nm for R3. The diffuse diffraction patterns observed indicate a mixture of phases, with the diffusivity attributed to the presence of an amorphous calcium phosphate phase in addition to crystalline HA. This mix of crystalline and amorphous calcium phosphate is consistent with the reported crystal structure for bone-derived mineral.[60] No differences in crystal structure were found between the mineralized interface and bone regions, or between immature and mature groups, which suggests that the formation of mineralized fibrocartilage and bone occur under similar biochemical environments and that the crystal structure is maintained over time.

Mineral maturity describes the progressive transformation of nonapatitic domains into well-crystallized apatites,[61] and from the IR spectra, it can be assessed by calculating the ratio of the 1030 cm^{-1} peak, which is indicative of apatitic phosphate in stoichiometric HA, and the 1020 cm^{-1} peak, which represents nonstoichiometric apatites.[22,42] Mineral crystallinity was found to be significantly higher in the bone region compared to the interface region in both immature and mature groups. It has been shown that crystallinity within the mineralized fibrocartilage region of the tendon-to-bone enthesis is affected by mechanical loading.[62] Therefore, the difference in mineral crystallinity between the interface and bone regions may be indicative of inherently different loads sustained within each of these tissue regions. No differences in mineral crystallinity were observed between the immature and mature ACL-to-bone insertions, however. It has been shown in a mouse model that a mineral gradient is established at the supraspinatus tendon-to-bone insertion within days after birth and that while carbonate content of apatite mineral at the enthesis increases over time, no significant difference in mineral crystallinity is detected.[63] These findings suggest that the mineralized matrix is essential for interface function and is therefore established and optimized early on in development. Indeed, it has been proposed that mineral at the developing enthesis helps to amplify and transduce mechanical signals for the induction of cell-mediated mineralization.[64] However, age-related changes in mineral crystallinity and maturity are well-established in bone and have been correlated with decreasing mechanical properties over time.[41,61] The age of the mature animals used in this study corresponds to approximately 18−30 human years of age,[56] which, while still relatively young, represents the age range of the majority of patients undergoing ACL reconstruction.[65] Future studies will evaluate the interface in older animals and the effects of degeneration on mineral crystallinity.

Comparison of the structure and organization of the ACL-to-bone insertion in juvenile and adult models suggests that matrix structure across the enthesis continues to change postnatally in response to these mechanical cues. It is well established that physiological loading plays a critical role in enthesis development,[66,67] and studies of rat cruciate ligament enthesis development reported that these changes can yield a multifold increase in tissue stiffness.[54] Furthermore, the spatial differences in matrix structure observed across the insertion contribute to progressive changes in mechanical properties across the enthesis[8] and reflect adaptions to the complex forces generated at the ligament-to-bone junction. This graded organization minimizes the formation of stress concentrations and facilitates the secure attachment of mechanically dissimilar tissues.

It is noted that there are limitations to this study related to the use of a quadrupedal animal model. Like all animal models, the bovine knee does not perfectly replicate the biomechanics or anatomy of the human knee. The passive range of motion of the bovine knee is limited compared to that of the human knee,[33] and the knee joints of quadrupedal animals are subject to different loading profiles than those of bipedal humans. Thus, there may be species-related differences in matrix structure due to differences in load distribution across the joint. Nevertheless, it has also been shown that the ACL is a primary force contributor in both quadruped and human knee movement[68] and despite differences in knee kinematics, the ACL is subject to significant loading in both cattle and humans

DOI: 10.1021/acsbiomaterials.6b00602
ACS Biomater. Sci. Eng. XXXX, XXX, XXX−XXX

and therefore likely undergo similar postnatal remodeling. Additionally, the bovine ACL more closely approximates the human ACL in terms of size and proportion than most other commonly used animal models.[33] Another challenge in this study was the analysis of only two-dimensional images of the insertion, which is a three-dimensional structure. While OCT can provide three-dimensional imaging of tissues, limitations in data processing capabilities restricted analysis to only one representative image for each sample volume. Future work will therefore focus on optimizing methods to process these three-dimensional data sets to enable analysis of matrix structural properties through the full three-dimensional volume of the ACL-to-bone insertion. Furthermore, these functional imaging methods can be coupled with mechanical testing methods to elucidate structure−function relationships across the immature and mature insertions.

This study is the first to systematically quantify the ultrastructural and microstructural properties of the ACL-to-bone interface, and, moreover, to examine how these properties change as a function of age. Collectively, these findings may be used to guide current efforts to develop biomimetic grafts for interface tissue engineering and integrative soft tissue repair. Specifically, the results from this study suggest that some matrix parameters, such as fibrous matrix organization and structure, can be expected to be optimized in *in vivo* postimplantation. However, other parameters, such as mineral distribution and crystal structure, are highly conserved with age and must be pre-established as part of the scaffold design. The age-related changes in tissue structure also underscore the importance of physiologic loading in enthesis maturation and indicate that mechanical stimulation may also be harnessed to guide tissue regeneration.

CONCLUSIONS

In summary, significant changes in collagenous matrix structure and organization occur during maturation of the ACL-to-bone insertion, while mineral distribution and crystal structure are largely conserved. These region- and age-dependent differences reflect adaptations to the complex loads sustained at the enthesis. This study enhances the current understanding of the structure−function relationships at soft tissue-to-bone interfaces, and provides key benchmark measures for integrative and functional ACL reconstruction and regeneration.

AUTHOR INFORMATION

Corresponding Author

*Phone: 212-854-4071. Fax: 212-854-8725. E-mail: hhlu@columbia.edu.

ORCID

Helen H. Lu: 0000-0002-6488-2060

Funding

This work was supported by the Presidential Early Career Award for Scientists and Engineers (to H.H.L.), the National Institutes of Health (5R01AR055280 (to H.H.L.), T32AR059038 (to D.Q.), and 1DP2HL127776-01 (to C.P.H.)), and used resources of the Center for Functional Nanomaterials, which is a U.S. DOE Office of Science Facility, at Brookhaven National Laboratory under Contract No. DE-SC0012704

Notes

The authors declare no competing financial interest.

ACKNOWLEDGMENTS

We acknowledge Christopher Aswin Hermawi and Jiaqi Guo for their help in OCT data acquisition, Dr. Jeffrey P. Spalazzi, Dr. Adele L. Boskey, and Dr. Nancy Pleshko for their help in FTIRI data acquisition and analysis, and Dr. I-Ning E. Wang for her help in histology.

REFERENCES

(1) Woo, S. L.; Buckwalter, J. A. AAOS/NIH/ORS Workshop. Injury and Repair of the Musculoskeletal Soft Tissues. Savannah, Georgia, June 18−20, 1987. *J. Orthop. Res.* **1988**, *6* (6), 907−931.

(2) Cooper, R. R.; Misol, S. Tendon and Ligament Insertion. A Light and Electron Microscopic Study. *J. Bone Joint Surg. Am.* **1970**, *52* (1), 1−170.

(3) Benjamin, M.; Evans, E. J.; Copp, L. The Histology of Tendon Attachments to Bone in Man. *J. Anat.* **1986**, *149*, 89−100.

(4) Benjamin, M.; Ralphs, J. R. Fibrocartilage in Tendons and Ligaments - an Adaptation to Compressive Load. *J. Anat.* **1998**, *193*, 481−494.

(5) Petersen, W.; Tillmann, B. Structure and Vascularization of the Cruciate Ligaments of the Human Knee Joint. *Anat. Embryol.* **1999**, *200* (3), 325−334.

(6) Niyibizi, C.; Visconti, C. S.; Gibson, G.; Kavalkovich, K. Identification and Immunolocalization of Type X Collagen at the Ligament-Bone Interface. *Biochem. Biophys. Res. Commun.* **1996**, *222* (2), 584−589.

(7) Wang, I. E.; Mitroo, S.; Chen, F. H.; Lu, H. H.; Doty, S. B. Age-Dependent Changes in Matrix Composition and Organization at the Ligament-to-Bone Insertion. *J. Orthop. Res.* **2006**, *24* (8), 1745−1755.

(8) Moffat, K. L.; Sun, W. H.; Pena, P. E.; Chahine, N. O.; Doty, S. B.; Ateshian, G. A.; Hung, C. T.; Lu, H. H. Characterization of the Structure-Function Relationship at the Ligament-to-Bone Interface. *Proc. Natl. Acad. Sci. U. S. A.* **2008**, *105* (23), 7947−7952.

(9) Friedman, M. J.; Sherman, O. H.; Fox, J. M.; Del Pizzo, W.; Snyder, S. J.; Ferkel, R. J. Autogeneic Anterior Cruciate Ligament (ACL) Anterior Reconstruction of the Knee. A Review. *Clin. Orthop. Relat. Res.* **1985**, *196*, 9−14.

(10) Robertson, D. B.; Daniel, D. M.; Biden, E. Soft Tissue Fixation to Bone. *Am. J. Sports Med.* **1986**, *14* (5), 398−403.

(11) Getelman, M. H.; Friedman, M. J. Revision Anterior Cruciate Ligament Reconstruction Surgery. *J. Am. Acad. Orthop. Surg* **1999**, *7* (3), 189−198.

(12) American Orthopaedic Society for Sports Medicine. Allografts in Sports Medicine: What Do We Know, Need to Know, and Need to Do? Round Table Discussion, 2006, Park City, UT.

(13) Vavken, P.; Murray, M. M. Translational Studies in Anterior Cruciate Ligament Repair. *Tissue Eng., Part B* **2010**, *16* (1), 5−11.

(14) Visconti, C. S.; Kavalkovich, K.; Wu, J.; Niyibizi, C. Biochemical Analysis of Collagens at the Ligament-Bone Interface Reveals Presence of Cartilage-Specific Collagens. *Arch. Biochem. Biophys.* **1996**, *328* (1), 135−142.

(15) Zhao, L.; Thambyah, A.; Broom, N. D. A Multi-Scale Structural Study of the Porcine Anterior Cruciate Ligament Tibial Enthesis. *J. Anat.* **2014**, *224* (6), 624−633.

(16) Gao, J.; Messner, K. Quantitative Comparison of Soft Tissue-Bone Interface at Chondral Ligament Insertions in the Rabbit Knee Joint. *J. Anat* **1996**, *188* (Pt 2), 367−373.

(17) Drexler, W.; Fujimoto, J. G. *Optical Coherence Tomography: Technology and Applications*; Springer Science & Business Media: Berlin, Germany, 2008.

(18) Klyen, B. R.; Shavlakadze, T.; Radley-Crabb, H. G.; Grounds, M. D.; Sampson, D. D. Identification of Muscle Necrosis in the Mdx Mouse Model of Duchenne Muscular Dystrophy Using Three-Dimensional Optical Coherence Tomography. *J. Biomed. Opt.* **2011**, *16* (7), 076013.

(19) Gan, Y.; Fleming, C. P. Extracting Three-Dimensional Orientation and Tractography of Myofibers Using Optical Coherence Tomography. *Biomed. Opt. Express* **2013**, *4* (10), 2150−2165.

DOI: 10.1021/acsbiomaterials.6b00602
ACS Biomater. Sci. Eng. XXXX, XXX, XXX−XXX

(20) Fleming, C. P.; Ripplinger, C. M.; Webb, B.; Efimov, I. R.; Rollins, A. M. Quantification of Cardiac Fiber Orientation Using Optical Coherence Tomography. *J. Biomed. Opt.* **2008**, *13* (3), 030505.
(21) Gan, Y.; Yao, W.; Myers, K. M.; Vink, J. Y.; Wapner, R. J.; Hendon, C. P. Analyzing Three-Dimensional Ultrastructure of Human Cervical Tissue Using Optical Coherence Tomography. *Biomed. Opt. Express* **2015**, *6* (4), 1090−1108.
(22) Kim, M.; Bi, X.; Horton, W. E.; Spencer, R. G.; Camacho, N. P. Fourier Transform Infrared Imaging Spectroscopic Analysis of Tissue Engineered Cartilage: Histologic and Biochemical Correlations. *J. Biomed. Opt.* **2005**, *10* (3), 031105.
(23) Bi, X.; Yang, X.; Bostrom, M. P.; Camacho, N. P. Fourier Transform Infrared Imaging Spectroscopy Investigations in the Pathogenesis and Repair of Cartilage. *Biochim. Biophys. Acta, Biomembr.* **2006**, *1758* (7), 934−941.
(24) Khanarian, N. T.; Boushell, M. K.; Spalazzi, J. P.; Pleshko, N.; Boskey, A. L.; Lu, H. H. FTIR-I Compositional Mapping of the Cartilage-to-Bone Interface As a Function of Tissue Region and Age. *J. Bone Miner. Res.* **2014**, *29*, 2643.
(25) Neurath, M. F.; Printz, H.; Stofft, E. Cellular Ultrastructure of the Ruptured Anterior Cruciate Ligament: A Transmission Electron Microscopic and Immunohistochemical Study in 55 Cases. *Acta Orthop. Scand.* **1994**, *65* (1), 71−76.
(26) Strocchi, R.; De Pasquale, V.; Facchini, A.; Raspanti, M.; Zaffagnini, S.; Marcacci, M. Age-Related Changes in Human Anterior Cruciate Ligament (ACL) Collagen Fibrils. *Ital J. Anat Embryol* **1996**, *101* (4), 213−220.
(27) Hefti, F. L.; Kress, A.; Fasel, J.; Morscher, E. W. Healing of the Transected Anterior Cruciate Ligament in the Rabbit. *J. Bone Joint Surg. Am.* **1991**, *73* (3), 373−383.
(28) Murray, M. M.; Magarian, E. M.; Harrison, S. L.; Mastrangelo, A. N.; Zurakowski, D.; Fleming, B. C. The Effect of Skeletal Maturity on Functional Healing of the Anterior Cruciate Ligament. *J. Bone Joint Surg. Am.* **2010**, *92* (11), 2039−2049.
(29) Noyes, F. R.; Grood, E. S. The Strength of the Anterior Cruciate Ligament in Humans and Rhesus Monkeys. *J. Bone Joint Surg. Am.* **1976**, *58* (8), 1074−1082.
(30) Woo, S. L.; Hollis, J. M.; Adams, D. J.; Lyon, R. M.; Takai, S. Tensile Properties of the Human Femur-Anterior Cruciate Ligament-Tibia Complex. The Effects of Specimen Age and Orientation. *Am. J. Sports Med.* **1991**, *19* (3), 217−225.
(31) Benjamin, M.; Tyers, R. N.; Ralphs, J. R. Age-Related Changes in Tendon Fibrocartilage. *J. Anat.* **1991**, *179*, 127−136.
(32) Legnani, C.; Terzaghi, C.; Borgo, E.; Ventura, A. Management of Anterior Cruciate Ligament Rupture in Patients Aged 40 Years and Older. *J. Orthop. Traumatol.* **2011**, *12* (4), 177−184.
(33) Proffen, B. L.; McElfresh, M.; Fleming, B. C.; Murray, M. M. A Comparative Anatomical Study of the Human Knee and Six Animal Species. *Knee.* **2012**, *19* (4), 493−499.
(34) Spalazzi, J. P.; Boskey, A. L.; Pleshko, N.; Lu, H. H. Quantitative Mapping of Matrix Content and Distribution Across the Ligament-to-Bone Insertion. *PLoS One* **2013**, *8* (9), e74349.
(35) Spalazzi, J. P.; Gallina, J.; Fung-Kee-Fung, S. D.; Konofagou, E. E.; Lu, H. H. Elastographic Imaging of Strain Distribution in the Anterior Cruciate Ligament and at the Ligament-Bone Insertions. *J. Orthop. Res.* **2006**, *24* (10), 2001−2010.
(36) Shadwick, R. E. Elastic Energy Storage in Tendons: Mechanical Differences Related to Function and Age. *J. Appl. Physiol.* **1990**, *68* (3), 1033−1040.
(37) de Carvalho, H. F.; Vidal, B. C. Structure and Histochemistry of a Pressure-Bearing Tendon of the Frog. *Ann. Anat.* **1994**, *176* (2), 161−170.
(38) Tuite, D. J.; Renstrom, P. A.; O'Brien, M. The Aging Tendon. *Scand. J. Med. Sci. Sports* **1997**, *7* (2), 72−77.
(39) Ghosh, P.; Taylor, T. K. The Knee Joint Meniscus. A Fibrocartilage of Some Distinction. *Clin. Orthop. Relat. Res.* **1987**, *224*, 52−63.
(40) Esquisatto, M. A.; Joazeiro, P. P.; Pimentel, E. R.; Gomes, L. The Effect of Age on the Structure and Composition of Rat Tendon Fibrocartilage. *Cell Biol. Int.* **2007**, *31* (6), 570−577.
(41) Akkus, O.; Adar, F.; Schaffler, M. B. Age-Related Changes in Physicochemical Properties of Mineral Crystals Are Related to Impaired Mechanical Function of Cortical Bone. *Bone* **2004**, *34* (3), 443−453.
(42) Paschalis, E. P.; DiCarlo, E.; Betts, F.; Sherman, P.; Mendelsohn, R.; Boskey, A. L. FTIR Microspectroscopic Analysis of Human Osteonal Bone. *Calcif. Tissue Int.* **1996**, *59* (6), 480−487.
(43) Dickinson, G. R. Chemical Fixation and the Preparation of Calcified Tissues for Transmission Electron Microscopy. In *Methods of Calcified Tissue Preparation*; Dickinson, G. R., Ed.; Elsevier: Amsterdam, The Netherlands, 1984; pp 79−148.
(44) *PDF-4+ 2010 (Database)*; International Centre for Diffraction Data: Newtown Square, PA, 2010.
(45) Fultz, B.; Howe, J. M. *Transmission Electron Microscopy and Diffractometry of Materials*, 4th ed.; Springer: Berlin, Germany, 2012;.
(46) Lake, S. P.; Miller, K. S.; Elliott, D. M.; Soslowsky, L. J. Effect of Fiber Distribution and Realignment on the Nonlinear and Inhomogeneous Mechanical Properties of Human Supraspinatus Tendon Under Longitudinal Tensile Loading. *J. Orthop. Res.* **2009**, *27* (12), 1596.
(47) Quinn, K. P.; Winkelstein, B. A. Preconditioning Is Correlated With Altered Collagen Fiber Alignment in Ligament. *J. Biomech. Eng.* **2011**, *133* (6), 064506.
(48) Miller, K. S.; Connizzo, B. K.; Soslowsky, L. J. Collagen Fiber Re-Alignment in a Neonatal Developmental Mouse Supraspinatus Tendon Model. *Ann. Biomed. Eng.* **2012**, *40* (5), 1102−1110.
(49) Parry, D. A.; Craig, A. S. Quantitative Electron Microscope Observations of the Collagen Fibrils in Rat-Tail Tendon. *Biopolymers* **1977**, *16* (5), 1015−1031.
(50) Parry, D. A.; Barnes, G. R.; Craig, A. S. A Comparison of the Size Distribution of Collagen Fibrils in Connective Tissues As a Function of Age and a Possible Relation Between Fibril Size Distribution and Mechanical Properties. *Proc. R. Soc. London, Ser. B* **1978**, *203* (1152), 305−321.
(51) Parry, D. A. The Molecular and Fibrillar Structure of Collagen and Its Relationship to the Mechanical Properties of Conncetive Tissue. *Biophys. Chem.* **1988**, *29*, 195−209.
(52) Erisken, C.; Zhang, X.; Moffat, K. L.; Levine, W. N.; Lu, H. H. Scaffold Fiber Diameter Regulates Human Tendon Fibroblast Growth and Differentiation. *Tissue Eng., Part A* **2013**, *19* (3−4), 519−528.
(53) Woo, S. L.; Ohland, K. J.; Weiss, J. A. Aging and Sex-Related Changes in the Biomechanical Properties of the Rabbit Medial Collateral Ligament. *Mech. Ageing Dev.* **1990**, *56* (2), 129−142.
(54) Messner, K. Postnatal Development of the Cruciate Ligament Insertions in the Rat Knee. Morphological Evaluation and Immunohistochemical Study of Collagens Types I and II. *Cells Tissues Organs* **1997**, *160* (4), 261−268.
(55) Parry, D. A.; Craig, A. S. Collagen Fibrils and Elastic Fibers in Rat-Tail Tendon: an Electron Microscopic Investigation. *Biopolymers* **1978**, *17* (4), 843−845.
(56) Kilborn, S. H.; Trudel, G.; Uhthoff, H. Review of Growth Plate Closure Compared With Age at Sexual Maturity and Lifespan in Laboratory Animals. *Contemp. Top. Lab Anim Sci.* **2002**, *41* (5), 21−26.
(57) Wood, G. C.; Keech, M. K. The Formation of Fibrils From Collagen Solutions. The Effect of Experimental Conditions: Kinetic and Electron Microscope Studies. *Biochem. J.* **1960**, *75*, 588−598.
(58) Genin, G. M.; Kent, A.; Birman, V.; Wopenka, B.; Pasteris, J. D.; Marquez, P. J.; Thomopoulos, S. Functional Grading of Mineral and Collagen in the Attachment of Tendon to Bone. *Biophys. J.* **2009**, *97* (4), 976−985.
(59) Liu, Y. X.; Thomopoulos, S.; Birman, V.; Li, J. S.; Genin, G. M. Bi-Material Attachment through a Compliant Interfacial System at the Tendon-to-Bone Insertion Site. *Mech. Mater.* **2012**, *44*, 83.
(60) Osborn, J. F.; Newesely, H. The Material Science of Calcium-Phosphate Ceramics. *Biomaterials* **1980**, *1* (2), 108−111.

DOI: 10.1021/acsbiomaterials.6b00602
ACS Biomater. Sci. Eng. XXXX, XXX, XXX−XXX

(61) Farlay, D.; Panczer, G.; Rey, C.; Delmas, P. D.; Boivin, G. Mineral Maturity and Crystallinity Index Are Distinct Characteristics of Bone Mineral. *J. Bone Miner. Metab.* **2010**, *28* (4), 433−445.
(62) Schwartz, A. G.; Lipner, J. H.; Pasteris, J. D.; Genin, G. M.; Thomopoulos, S. Muscle Loading Is Necessary for the Formation of a Functional Tendon Enthesis. *Bone* **2013**, *55* (1), 44−51.
(63) Schwartz, A. G.; Pasteris, J. D.; Genin, G. M.; Daulton, T. L.; Thomopoulos, S. Mineral Distributions at the Developing Tendon-to-Bone Enthesis. *PLoS One* **2012**, *7* (11), e48630.
(64) Liu, Y.; Schwartz, A. G.; Birman, V.; Thomopoulos, S.; Genin, G. M. Stress Amplification During Development of the Tendon-to-Bone Attachment. *Biomech. Model. Mechanobiol.* **2014**, *13* (5), 973−983.
(65) Mall, N. A.; Chalmers, P. N.; Moric, M.; Tanaka, M. J.; Cole, B. J.; Bach, B. R., Jr.; Paletta, G. A., Jr. Incidence and Trends of Anterior Cruciate Ligament Reconstruction in the United States. *Am. J. Sports Med.* **2014**, *42* (10), 2363−2370.
(66) Niyibizi, C.; Visconti, C. S.; Kavalkovich, K.; Woo, S. L. Collagens in an Adult Bovine Medial Collateral Ligament: Immunofluorescence Localization by Confocal Microscopy Reveals That Type XIV Collagen Predominates at the Ligament-Bone Junction. *Matrix Biol.* **1995**, *14* (9), 743−751.
(67) Thomopoulos, S.; Kim, H. M.; Rothermich, S. Y.; Biederstadt, C.; Das, R.; Galatz, L. M. Decreased Muscle Loading Delays Maturation of the Tendon Enthesis During Postnatal Development. *J. Orthop. Res.* **2007**, *25* (9), 1154−1163.
(68) Nesbitt, R. J.; Herfat, S. T.; Boguszewski, D. V.; Engel, A. J.; Galloway, M. T.; Shearn, J. T. Primary and Secondary Restraints of Human and Ovine Knees for Simulated in Vivo Gait Kinematics. *J. Biomech.* **2014**, *47* (9), 2022−2027.

DOI: 10.1021/acsbiomaterials.6b00602
ACS Biomater. Sci. Eng. XXXX, XXX, XXX−XXX